Josephson diode effect in a line-centered honeycomb lattice based superconductor junction

Ya-Jun Wei,[1] Juan-Juan Wang,[2] and J. Wang[1,*]
[1]*School of Physics, Southeast University, Nanjing 210096, China*
[2]*Department of Physics, College of Sciences, Nanjing Agricultural University, Nanjing, Jiangsu 210095, China*

(Received 13 November 2022; revised 25 June 2023; accepted 9 August 2023; published 23 August 2023)

The Josephson diode effect (JDE) is the asymmetry of the critical supercurrent flowing along opposite current directions. We study a mechanism in this work to generate a possible JDE in the two-dimensional line-centered honeycomb (LCH) lattice based Josephson junction in which the supercurrent flows via the topological edge states. Since the two helical edge states of the LCH topological insulator have different Fermi velocities, the field-free Josephson junction is shown to exhibit a spin-resolved JDE in which the critical supercurrent is asymmetric over the two opposite current directions for each spin species. By introducing magnetization in the circuit, a charge version of JDE occurs in the system.

DOI: 10.1103/PhysRevB.108.054521

I. INTRODUCTION

For the past few decades, Josephson junctions (JJs) have attracted much attention from researchers, both from a fundamental physics point of view and for potential applications in superconducting electronics [1–21]. For example, the π state JJ was proposed as circuit elements for quantum computation and as on-chip π phase shifters or π batteries for various self-biasing quantum/classical circuits [22–26]. Recently, the superconducting rectification effect was observed experimentally in superconductor films [27–29] and has ignited huge research interest in this field [30–48] because it undoubtedly possesses significant application potential for the fabrication of superconducting electronic devices. As is known, the semiconducting diode (*p-n* junction) is already one of the key devices of the modern semiconductor industry, although there are some advantages envisaged for the superconducting diode like zero-voltage resistance, high-speed switching, and low noise because it has very low resistance when operated at cryogenic temperatures. In addition, superconducting diodes can also be used as qubits in quantum computing and as detectors of electromagnetic radiation in applications [49].

Generally, it is believed that the magnetic field together with the lack of an inversion center in the superconductor system gives rise to nonreciprocal supercurrents; that is, the forward critical supercurrent is not equal to the backward (reversal) one. Therefore, a charge current with a magnitude between them might be in a nonresistive state flowing in one direction but dissipative in the opposite direction. Broken time-reversal symmetry or inversion symmetry of the system is among the preconditions of the superconducting diode. The magnetic field and the spin-orbit interaction are taken into account in reality. The first superconducting diode effect was observed in a $[Nb/V/Ta]_n$ superlattice by Ando *et al.* [27], and afterwards, a number of experimental works confirmed this effect in junction-free superconductors [30–32]. Bauriedl *et al.* [28] first measured the JJ version of the superconducting diode in the Al/InAs–two-dimensional electron gas/Al junction. Interest in the superconducting diode has been further advanced by the recent demonstration in unconventional/topological superconducting materials. For instance, the diode effect was also observed in unconventional superconductors such as magic-angle-twisted bilayer graphene [31]. It was also demonstrated in topological superconductors in which superconductivity coexists with nontrivial band topology, e.g., topological JJs where the type-II Dirac semimetal $NiTe_2$ is sandwiched between the conventional *s*-wave spin-singlet superconductor Nb [50].

In theoretic aspects, Daido *et al.* [35] showed that the intrinsic mechanism of the junction-free superconductors causing the diode effect was due to the nonreciprocity of depairing critical current by employing mean-field, Bogoliubov–de Gennes, and Ginzburg-Landau theories. However, in the engineered junction's diode, Davydova *et al.* [51] showed that the physics mechanism is from both the Doppler energy shift in the Andreev bound states due to continuum momentum Cooper pairing and the asymmetric current from the continuum of states due to the phase-independent contribution. The JJ version of the diode termed the Josephson diode effect (JDE) was also demonstrated successfully in experiments and even identified without any application of magnetic field [47,50–57]. The physics is clear that the Josephson high-order harmonics leads to the JDE within the high junction's transparency [32] when the inversion symmetry of the junction is broken. In some works [58,59], the broken time-reversal symmetry could come from the valley polarization in the monolayer graphene or multilayer graphene-based JJ instead of the spin polarization from the magnetic field or magnetization. Nevertheless, a method providing an effective and clear means to improve and control the JDE is urgently needed in this field.

In this work, we demonstrate that the spin-related JDE can appear in a field-free JJ based on the exotic helical edge

*jwang@seu.edu.cn

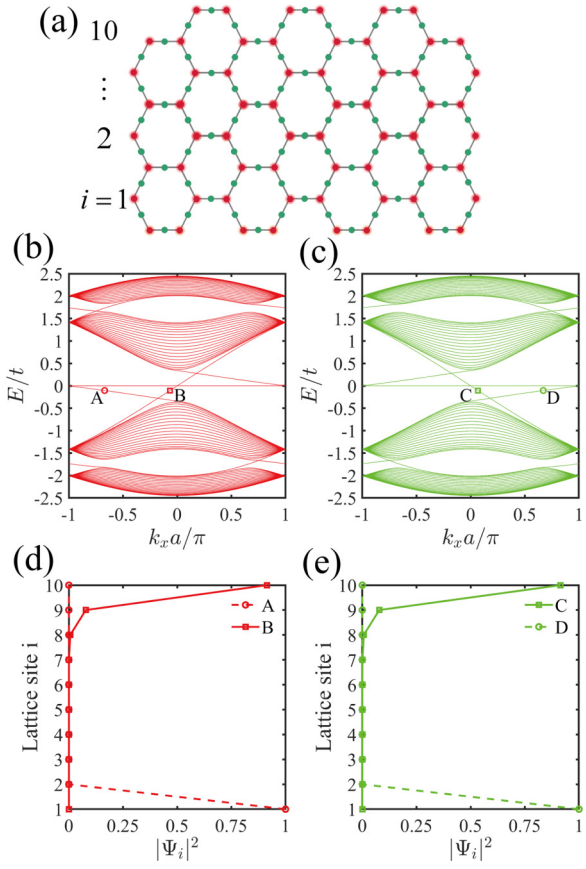

FIG. 1. (a) Schematic of the line-centered honeycomb lattice. Electronic band structures of the LCH nanoribbon with SOC for the (b) spin-up and (c) spin-down species. (d) and (e) The wave function distribution Ψ_i of the edge states marked in (b) and (c) on the transverse ribbon site i. Parameters are $\lambda = 0.1t$ and the number of unit cells $N_y = 10$.

states of a two-dimensional (2D) topological insulator, the bis(iminothiolato)nickel monolayer lattice [60,61], which has a line-centered honeycomb lattice (LCH) structure, as shown in Fig. 1(a). It is found that, due to the flat band in the LCH system, there are two helical edge states possessing very different Fermi velocities and the superconducting quasiparticles in the two states will accumulate a different phase shift so that the spin-related JDE can arise in the JJ. Moreover, a charge JDE is possible with the introduction of magnetization to the system. This mechanism for the JDE cannot be found in traditional topological insulator-based JJs like the Kane-Mele quantum spin Hall insulator [62].

This work is organized in the following manner. In Sec. II, we describe the model Hamiltonian of the LCH lattice based JJ. In Sec. III, the spin-related JDE in both the continuum model and the lattice model is discussed, along with the possible charge JDE. The conclusions are briefly summarized in the last section.

II. MODEL

Let us start with the exotic topological edge states constructed in the monolayer lattice of the 2D LCH material bis(iminothiolato)nickel [$Ni_3C_{12}(NH)_6S_6$] [60,61]. As schematically shown in Fig. 1(a), the LCH model is like the graphene lattice but has an extra atom residing on each hexagon edge and can be regarded as a hybrid of a honeycomb sublattice and a kagome sublattice. The LCH lattice exhibits a nontrivially topological band structure when an intrinsic spin-orbit coupling (SOC) interaction is considered, so the exotic topological edge states appear. We now consider a finite-size LCH nanoribbon to explain the exotic edge states, and the ribbon lattice is described by

$$H = -t\sum_{\langle ij\rangle\sigma} c^{\dagger}_{i\sigma}c_{j\sigma} + i\lambda \sum_{\langle\langle i,j\rangle\rangle\alpha,\beta} v_{ij}c^{\dagger}_{i\alpha}\sigma_{\alpha,\beta}c_{j\beta}, \qquad (1)$$

where the first term is the nearest-neighbor hopping with strength t. λ represents the amplitude of the next-nearest-neighbor SOC. $v_{ij} = \vec{d^1_{i,j}} \times \vec{d^2_{i,j}} = +(-)1$ when the next-nearest-neighbor hopping is clockwise (counterclockwise) with respect to the LCH sheet. $\vec{d^1_{i,j}}$ and $\vec{d^2_{i,j}}$ are the two unit vectors along the nearest-neighbor bonds connecting site i to its next-nearest neighbor j, and $\vec{\sigma}$ is the vector of the Pauli spin matrices.

The energy band of the LCH lattice nanoribbon is presented in Figs. 1(b) and 1(c) for the spin-up and -down species, respectively. As we can see, there are three curves with different slopes of the linear $E - k$ dispersions across the bulk energy gap beside the flat band lying at the band center. The crossing points are at the Γ and **M** points of the Brillouin zone, representing different helical edge states. Note that there is only one Dirac point in the LCH model, and no valley degeneracy is present, unlike in the graphene case. In Figs. 1(d) and 1(e), the wave function distributions for the marked points in the energy band are plotted. The edge states of the B and C lines are the same as those in the Kane-Mele model [62] linking the valence and conduction bands, while the exotic edge states of the A and D lines connect the flat band with valence and/or conduction bands due to the topology of the flat band. Note that the two edge states at the upper and lower edges have different Fermi velocities, and this situation is very different from the usual Kane-Mele topological insulator [62].

As is known, the superconducting Cooper pairs will accumulate a dynamic phase when they propagate in the normal region (weak link) of the JJ, which is certainly related to the Fermi velocity; that is, different velocities of quasiparticles will lead to different dynamic phase accumulations and in turn affect the Andreev bound states (ABSs) of the JJ as well as the supercurrent. So we can devise a JJ by merely employing such exotic helical edge states as shown in Fig. 2, where two s-wave superconductor electrodes are deposited on the LCH lattice and only the edge states sustain the possible supercurrents. The Hamiltonian for such a JJ based on the exotic edge states is simply described as [64,65]

$$H_S = \begin{bmatrix} H_{u(l)} - \mu(x) & \Delta(x)e^{i\phi_{L(R)}} \\ \Delta(x)e^{-i\phi_{L(R)}} & \mu(x) - \mathcal{T}H_{u(l)}\mathcal{T}^{-1} \end{bmatrix}, \qquad (2)$$

where the Hamiltonian $H_u = \sigma_z \hbar v^u_f(k_x + \Gamma)$ for the upper helical edge state and $H_l = -\sigma_z \hbar v^l_f(k_x + \mathbf{M})$ for the lower helical edge states in the LCH ribbon, $v^{u(l)}_f$ denotes the Fermi velocity for the upper (lower) edge state, and σ_z is the Pauli spin matrix. $\Gamma = 0$ and $\mathbf{M} = \pm\pi/a$ represent the degeneracy

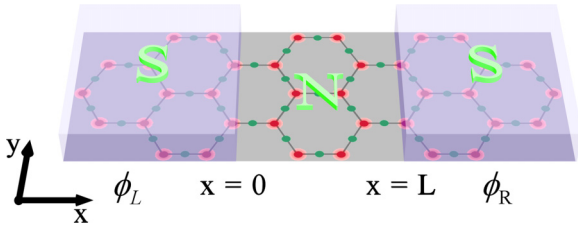

FIG. 2. Setup of the S/N/S JJ based on the LCH lattice, where N denotes the normal region of the JJ. S is formed by putting an s-wave superconductor onto the LCH nanoribbon structure. $\phi_{L(R)}$ denotes the left (right) superconducting phase.

or crossing points of the two edge states. k_x is an expanded small momentum quantity around Γ or $\mathbf{M}$. μ is the universal chemical potential, and $\Delta(x) = \Delta[\theta(x-L)+\theta(-x)]$ is limited in the left ($x<0$) and right ($x>L$) superconductor electrodes; $\phi_{L(R)}$ is the superconducting phase, $\theta(x)$ is a step function, and $\mathcal{T}$ denotes the time-reversal operator.

The ABS can be directly derived [64–66] (the details are shown in the Appendix):

$$E^{u(l)}_{\uparrow(\downarrow)} = \pm\Delta\cos\big(\phi/2 \pm \delta k_x^{u(l)} L/2\big), \tag{3}$$

where $\uparrow(\downarrow) = \pm$ denotes spin-up (spin-down) quasiparticles and $\delta k_x^{u(l)}$ is the wave number difference between electronlike and holelike quasiparticles for the upper edge states with $\delta k_x^u = \frac{2E^u}{\hbar v_f^u}$ and lower edge states with $\delta k_x^l = 2\pi - \frac{2E^l}{\hbar v_f^l}$. $\phi = \phi_R - \phi_L$ indicates the superconducting phase difference. Generally, one can present an analytic expression by assuming a short junction with $L \ll \xi$, with ξ being the superconducting coherence length. However, the velocity is quite small for the edge states connecting the flat band and conduction/valence band, so the dynamic phase accumulation $k_x^{u(l)}L$ can be significantly enlarged.

The ABS can carry a supercurrent as [59,65]

$$I = \sum_{u(l)} \frac{\partial E^{u(l)}}{\partial \phi} \tanh\big(\beta_T E^{u(l)}/2\big), \tag{4}$$

where β_T is the temperature factor. We now prepare to numerically calculate Eqs. (3) and (4) for the JJ supercurrent. In numerics, the pair potential is set as $\Delta = 10^{-3}t$, where the hopping integral t is set as an energy unit, $t = 1$. Since the mean-field BCS Hamiltonian is taken into account, the universal chemical potential is taken to be $\mu = 0.02t$, so that $\mu \gg \Delta$. The zero temperature is considered in this work, and no extra external bias or static potential is taken into account.

III. RESULTS AND DISCUSSION

A. Continuum model for spin JDE

For simplicity, the case of a spin-up electron pairing with a spin-down hole is considered, and the opposite pairing can be analyzed in the same way. By solving Eq. (3), we can obtain the numerical self-consistent ABS that is depicted in Fig. 3(a). It is seen that the ABS composed of lower edge states (dashed line) deviates severely from the negative cosine function. This occurs because the Fermi velocity of lower edge states v_f^l is so small that the large phase shift of the ABS is given by

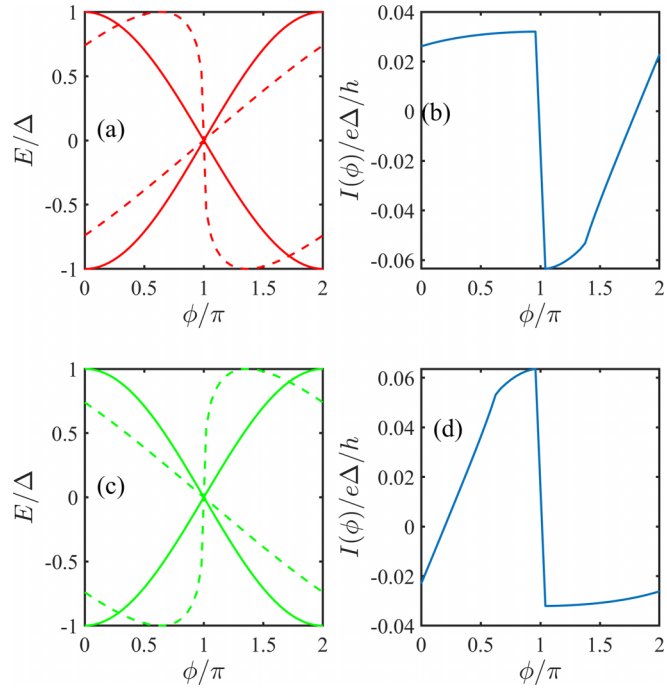

FIG. 3. The ABS as a function of the superconducting phase difference ϕ (a) for a spin-up electron pairing with a spin-down hole and (c) for a spin-down electron pairing with a spin-up hole and (b) and (d) the corresponding spin-related supercurrent versus the phase difference ϕ. Parameters are taken as $\lambda = 0.01t$ and $L = 10a$.

$\delta k_x^l L = (2\pi - \frac{2E^l}{\hbar v_f^l})L$. However, the phase shift of the ABS accumulated through the upper edge state is trivial due to the larger Fermi velocity v_f^u, as shown in Fig. 3(a) (solid line).

As a result of the electron chirality of the edge states, the electronlike quasiparticle at the upper edge is right going, and then the supercurrent originating from the spin-up electron pairing with a spin-down hole should be left going at the upper edge, which means that only the ABS satisfying the electron chirality carries the supercurrent. The ABS originating from lower edge states should contribute to only the right-going supercurrent. Therefore, one can acquire the supercurrent versus the phase difference ϕ by calculating the partial derivatives of the ABSs fulfilling the electron chirality, and the result is plotted in Fig. 3(b). It is shown that the critical supercurrent is asymmetric between the two opposite flowing directions. This is mainly attributed to the exotic edge states with different Fermi velocities. This mechanism is different from the usual JDE where the high harmonics of the Josephson current [32,58] plays a vital role.

Specifically, the ABS composed of upper edge states exhibits a slight phase shift $\delta k_x^u L = \frac{2E^u}{\hbar v_f^u} L$ due to the larger Fermi velocity v_f^u, and it is approximately a cosine function $[\cos(\phi/2)]$. As a result, the left-going supercurrent originating from this ABS has a sine function form, $I \sim \sin(\phi/2)$. However, owing to the large phase shift $\delta k_x^l L = 2\pi - \frac{2E^l}{\hbar v_f^l} L$, the ABS composed of the opposite lower edge states deviates severely from the negative cosine function. While at the band center $E \sim 0$, the phase shift $\delta k_x^l L = 2\pi - \frac{2E^l}{\hbar v_f^l} L$ vanishes due

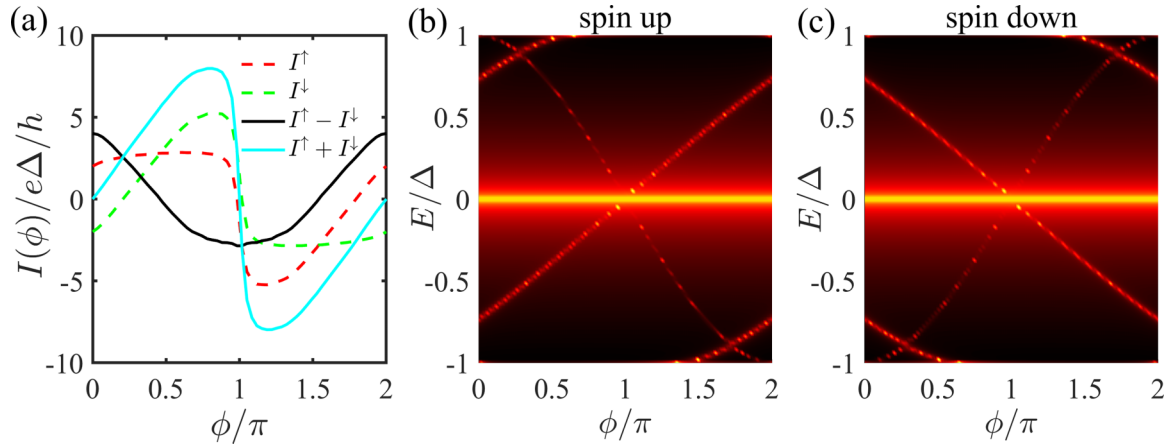

FIG. 4. (a) Spin-related supercurrent versus the phase difference ϕ, where $I^{\uparrow(\downarrow)}$ represents the supercurrent originating from a spin-up (spin-down) electron pairing with a spin-down (spin-up) hole. The spin-resolved particle density distribution in the superconducting energy gap as a function of ϕ within an arbitrary unit for (b) spin up and (c) spin down. The other parameters are the same as in Fig. 3.

to the electronlike and holelike quasiparticle energy bands crossing at the **M** point, as can be seen in Fig. 3(a). Consequently, the slope of the ABS $|\frac{\partial E^l}{\partial \phi}|$ is totally decreased. This means the reduced right-going supercurrent and the critical supercurrent are not equal to the left-going one; that is, the "spin-up" JDE arises. Nevertheless, the opposite "spin-down" JDE will appear when the spin-down electronlike quasiparticle pairing with the spin-up holelike quasiparticle is taken into account, as shown in Figs. 3(c) and 3(d). So the system does not show any charge JDE since the time-reversal symmetry has not been broken yet.

B. Lattice model for spin JDE

In this section, we calculate the supercurrent sustained by the exotic edge states within a lattice model to confirm the above findings based on the continuum model. The superconductivity in the left and right lattice leads in Fig. 2 is assumed from the superconducting proximity effect [63] and is described by [64,66]

$$H_{l(r)} = \sum_{i\sigma} \Delta \mathbf{e}^{i\phi_{l(r)}} c^{\dagger}_{i\sigma} c^{\dagger}_{i\bar{\sigma}} + \text{c.c.}, \tag{5}$$

where $\bar{\sigma} = -\sigma$, while the LCH band structure is still described by Eq. (1). The supercurrent can be worked out from [64,66]

$$I = \frac{e}{\hbar} \int \frac{dE}{2\pi} \text{Tr}[G^{<}_{l,l+1}(E)\widetilde{t}_{l+1,l} - \text{H.c.}], \tag{6}$$

where $G^{<}(E)$ is the lesser Green's function, the subscript l is the index of the unit slice of the nanoribbon lattice, $\widetilde{t}_{l+1,l}$ is the hopping matrix between the neighbor slices, and the trace is over the unit slice and electron space. At equilibrium, $G^{<} = [G^{a} - G^{r}]f(E)$, where $G^{r(a)}$ is the retarded (advanced) Green's function and f is the Fermi-Dirac distribution function. $G^{r(a)}$ is the retarded (advanced) Green's function in the lattice and Nambu space [59].

Figure 4(a) plots the spin-resolved $I(\phi)$ based on the above lattice model. $I^{\uparrow}(\phi)$ represents the spin-up electron pairing with the spin-down hole (red dashed line) and exhibits the spin-up JDE: the left- and right-going critical supercurrents are different. This behavior entirely recovers the result of the continuum model shown in Fig. 3(b). In Fig. 4(b), we also calculate the ABS in the superconducting energy gap, which is represented by the energy-resolved particle density distribution [64]. We can see that only the ABS fulfilling the electron chirality exists, which agrees with the practical ABS obtained in the continuum model, as shown in Fig. 3(a), while the missing ABS violates the chirality of the electron. The horizontal line is due to the flat band in the LCH lattice in Figs. 4(b) and 4(c).

The spin-down ABS is shown in Fig. 4(c) for the situation in which the spin-down electron pairs with the spin-up hole. Obviously, $I^{\downarrow}(\phi) = -I^{\uparrow}(-\phi)$ due to the time-reversal symmetry, so the spin-down supercurrent can exhibit the opposite JDE, as shown in Fig. 4(a). Therefore, we can see that the spin supercurrent $I_s = I_{\uparrow} - I_{\downarrow}$ displays a spin version JDE [black solid line in Fig. 4(a)], but there is no charge version JDE (blue solid line).

C. Charge JDE via magnetization

To obtain a charge JDE, we introduce magnetization into the JJ, which is assumed in the middle nonsuperconducting region of the JJ in Fig. 2. In the lattice model, it is simply described by $H_m = \sum_{i\sigma\sigma'} \sigma_z h_z c^{\dagger}_{i\sigma} c_{i\sigma'}$, where h_z is an energy unit that denotes the strength of the exchange field, σ and σ' are the spin indices, and σ_z is a Pauli operator. So the spin-up and spin-down subbands have an energy shift of h_z. We repeat the same calculations as those shown in Fig. 4, and the results are presented in Fig. 5. The antisymmetry between the corresponding spin-resolved supercurrents is broken, i.e., $I^{\downarrow}(\phi) \neq -I^{\uparrow}(-\phi)$, in Fig. 5 (red and green dashed lines). Consequently, the critical charge supercurrent $I^{\downarrow} + I^{\uparrow}$ is also asymmetric between the two opposite flowing directions, and a charge JDE arises.

In Fig. 6, we plot the charge JDE efficiency as a function of the strength of h_z for different lengths of the central nonsuperconducting region of the JJ L, and it is defined as [59]

$$\eta = \frac{|I_c^{+} - I_c^{-}|}{I_c^{+} + I_c^{-}}, \tag{7}$$

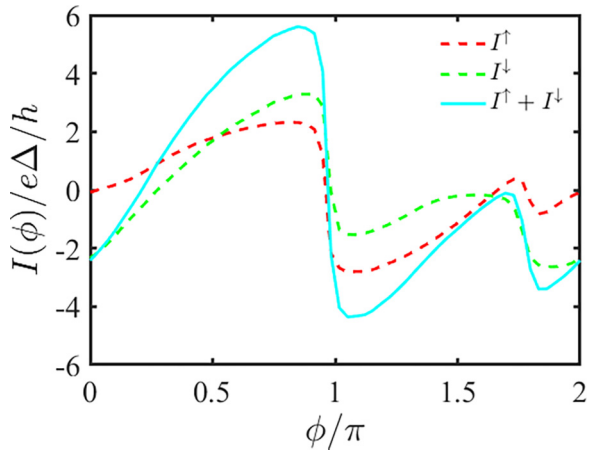

FIG. 5. Spin-related supercurrent versus the phase difference ϕ. Here, $h_z = 1.2\Delta$, and the other parameters are as in Fig. 3.

where $I_c^{+(-)}$ denotes the critical supercurrent for the right-going (left-going) one. Since the phase shift, the exchange field, and the length of the JJ can affect the JDE efficiency, the JDE is not linearly dependent on h_z except in the very weak h_z case. Owing to the spin-related JDE mainly from the different phase shifts of quasiparticles in the upper and lower edge states, h_z can certainly affect such a phase shift as well as the junction's transparency. Therefore, the charge JDE efficiency's dependence on h_z is very subtle and even exhibits some oscillations, as shown in Fig. 6.

We have exploited the two helical edge states of a topological insulator to construct a JJ based superconducting diode, and the crucial factor is the presence of a flat band which leads to the edge states possessing different Fermi velocities. The model device is feasible in experiments since there are many experimental works observing the topological superconductivity using the helical edge states of a topological insulator [67–70]. Similarly, there are also a lot of theoretical works studying the JJ based on the same model device using the two helical edge states of a topological insulator [71–73].

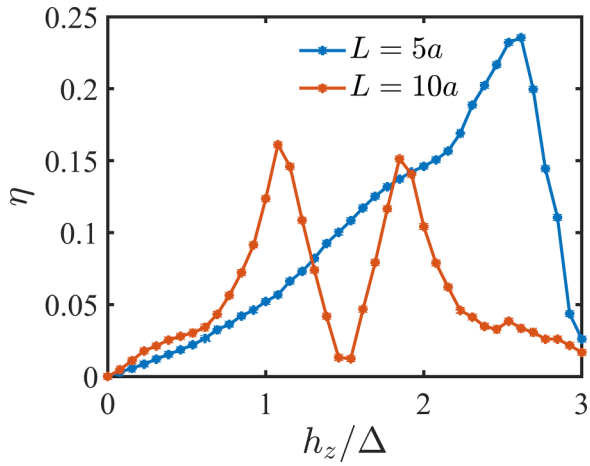

FIG. 6. JDE efficiency η as a function of the magnetization strength h_z for different lengths of the central region L. Other parameters are the same as in Fig. 3.

In Ref. [71], the authors achieved the JDE by exploiting the different velocities of the up and down helical edge states, but in our work, we do not apply any magnetic field and introduce an asymmetric inversion-breaking interaction that leads to the different velocities, which are, however, intrinsic in the topological insulator of the bis(iminothiolato)nickel monolayer lattice due to the flat band across the band center.

IV. CONCLUSION

In conclusion, we demonstrated that a devised JJ can give rise to a spin-related JDE when the usual JJ is based on the exotic helical edges of the LCH lattice topological insulator. Since the upper and lower helical edge states have different Fermi velocities of the electrons, the spin-resolved ABS has a contrasted phase shift, so the spin-resolved JDE can occur. By introducing an exchange field in the system, a charge version JDE was identified. Our finding provides a mechanism to generate the JDE.

The data that support the findings of this study are available within the paper.

ACKNOWLEDGMENTS

This work is supported financially by National Science Foundation of China (Grant No. 12174051).

APPENDIX: THE DERIVATION OF ANDREEV BOUND STATES

For simplicity, let us consider an superconductor normal metal superconductor (SNS) JJ employing upper edge states (a spin-up electronic state pairing with a spin-down hole state); the corresponding Bogoliubov–de Gennes equation can be written as [64,65]

$$\begin{bmatrix} \hbar v_F k_x^e - \mu(x) & \Delta(x)e^{i\phi_{L(R)}} \\ \Delta(x)e^{-i\phi_{L(R)}} & \mu(x) - \hbar v_F k_x^h \end{bmatrix} \begin{bmatrix} u_e \\ v_e \end{bmatrix} = E \begin{bmatrix} u_e \\ v_e \end{bmatrix}, \quad \text{(A1)}$$

where v_F denotes the Fermi velocity, μ is the universal chemical potential, $\Delta(x) = \Delta[\theta(x-L) + \theta(-x)]$ is limited in the left $(x < 0)$ and right $(x > L)$ superconductor electrodes, $\phi_{L(R)}$ is the superconducting phase, and $\theta(x)$ is a step function. We obtain the eigenstates in the N region by solving Eq. (8):

$$\Psi_e^+ = e^{ik_x^e x} \begin{bmatrix} 1 \\ 0 \end{bmatrix} \quad \text{(A2)}$$

and

$$\Psi_h^- = e^{ik_x^h x} \begin{bmatrix} 0 \\ 1 \end{bmatrix}, \quad \text{(A3)}$$

where Ψ_e^+ (Ψ_h^-) indicates the electron (hole) moves in the $+x$ ($-x$) direction. The wave vector $k_x^{e(h)} = \pm\frac{E}{\hbar v_F}$ is the longitudinal one of the electron (hole) quasiparticles. We consider the energy regime where $E < \Delta$, and the simplified wave functions in the two S regions are obtained as

$$\Psi_S^- = e^{ik_s^- x} \begin{bmatrix} \frac{E-i\Omega}{\Delta} e^{i\phi_L} \\ 1 \end{bmatrix} \quad \text{(A4)}$$

and

$$\Psi_S^+ = e^{ik_s^+ x}\begin{bmatrix}\frac{E+i\Omega}{\Delta}e^{i\phi_R}\\ 1\end{bmatrix}, \tag{A5}$$

where $\Omega = \sqrt{\Delta^2 - E^2}$ and $k_s^\pm = \pm i\Omega$. The wave functions in the N and two S regions are given by

$$\begin{aligned}\Psi_N &= t_e\Psi_e^+ + r_h\Psi_h^-,\\ \Psi_S^L &= r_s\Psi_S^-,\\ \Psi_S^R &= t_s\Psi_S^+,\end{aligned} \tag{A6}$$

where t_e, r_h, r_s, and t_s are the scatting amplitudes. Therefore, using the matching conditions at $x = 0$ and $x = L$,

$$\begin{aligned}\Psi_S^L|_{x=0} &= \Psi_N|_{x=0},\\ \Psi_N|_{x=L} &= \Psi_S^R|_{x=L},\end{aligned} \tag{A7}$$

we can obtain

$$\begin{aligned}r_s\begin{bmatrix}\frac{E-i\Omega}{\Delta}e^{i\phi_L}\\ 1\end{bmatrix} &= t_e\begin{bmatrix}1\\0\end{bmatrix} + r_h\begin{bmatrix}0\\1\end{bmatrix},\\ t_e e^{ik_x^e L}\begin{bmatrix}1\\0\end{bmatrix} + r_h e^{ik_x^h L}\begin{bmatrix}0\\1\end{bmatrix} &= t_s e^{ik_s^+ L}\begin{bmatrix}\frac{E+i\Omega}{\Delta}e^{i\phi_R}\\ 1\end{bmatrix}.\end{aligned} \tag{A8}$$

The ABS can be derived by solving the above quaternion system of first-order equations as [64]

$$\begin{aligned}E &= \pm\Delta\cos\left[\frac{1}{2}\left(k_x^e L - k_x^h L - \phi\right)\right]\\ &= \pm\Delta\cos\left[\frac{1}{2}(\delta k_x L - \phi)\right],\end{aligned} \tag{A9}$$

where $\delta k_x = k_x^e - k_x^h = \frac{2E}{\hbar v_F}$ and $\phi = \phi_L - \phi_R$.

[1] A. A. Golubov, M. Yu. Kupriyanov, and E. Il'ichev, Rev. Mod. Phys. **76**, 411 (2004).
[2] D. Monroe, M. Alidoust, and I. Žutić, Phys. Rev. Appl. **18**, L031001 (2022).
[3] A. Zyuzin, M. Alidoust, and D. Loss, Phys. Rev. B **93**, 214502 (2016).
[4] M. Alidoust and H. Hamzehpour, Phys. Rev. B **96**, 165422 (2017).
[5] M. Alidoust, M. Willatzen, and A.-P. Jauho, Phys. Rev. B **98**, 184505 (2018).
[6] P. E. C. Ashby and C. Kallin, Phys. Rev. B **79**, 224509 (2009).
[7] M. H. S. Amin, A. N. Omelyanchouk, and A. M. Zagoskin, Phys. Rev. B **63**, 212502 (2001).
[8] M. Alidoust, M. Willatzen, and A.-P. Jauho, Phys. Rev. B **98**, 085414 (2018).
[9] M. Alidoust, Phys. Rev. B **98**, 245418 (2018).
[10] M. Alidoust and K. Halterman, Phys. Rev. B **101**, 035120 (2020).
[11] M. Alidoust, Phys. Rev. B **101**, 155123 (2020).
[12] D. Sinha, Phys. Rev. B **102**, 085144 (2020).
[13] M. Alidoust, C. Shen, and I. Žutić, Phys. Rev. B **103**, L060503 (2021).
[14] A. Assouline, C. Feuillet-Palma 1, N. Bergeal, T. Zhang, A. Mottaghizadeh, A. Zimmers, E. Lhuillier, M. Eddrie, P. Atkinson, M. Aprili, and H. Aubin, Nat. Commun. **10**, 126 (2019).
[15] I. V. Bobkova, A. M. Bobkov, A. A. Zyuzin, and M. Alidoust, Phys. Rev. B **94**, 134506 (2016).
[16] D. M. Heim, N. G. Pugach, M. Y. Kupriyanov, E. Goldobin, D. Koelle, and R. Kleiner, J. Phys.: Condens. Matter **25**, 215701 (2013).
[17] E. Goldobin, D. Koelle, and R. Kleiner, Phys. Rev. B **91**, 214511 (2015).
[18] A. A. Mazanik, I. R. Rahmonov, A. E. Botha, and Y. M. Shukrinov, Phys. Rev. Appl. **14**, 014003 (2020).
[19] K. Kulikov, D. Sinha, Yu. M. Shukrinov, and K. Sengupta, Phys. Rev. B **101**, 075110 (2020).
[20] Y. M. Shukrinov, I. R. Rahmonov, and K. Sengupta, Phys. Rev. B **99**, 224513 (2019).
[21] H. Meng, X. Wu, Y. Ren, and J. Wu, Phys. Rev. B **106**, 174502 (2022).
[22] L. B. Ioffe, V. B. Geshkenbein, M. V. Feigel'man, A. L. Fauchère, and G. Blatter, Nature (London) **398**, 679 (1999).
[23] G. Blatter, V. B. Geshkenbein, and L. B. Ioffe, Phys. Rev. B **63**, 174511 (2001).
[24] A. V. Ustinov and V. K. Kaplunenko, J. Appl. Phys. **94**, 5405 (2003).
[25] T. Yamashita, K. Tanikawa, S. Takahashi, and S. Maekawa, Phys. Rev. Lett. **95**, 097001 (2005).
[26] A. K. Feofanov, V. A. Oboznov, V. V. Bol'ginov, J. Lisenfeld, S. Poletto, V. V. Ryazanov, A. N. Rossolenko, M. Khabipov, D. Balashov, A. B. Zorin, P. N. Dmitriev, V. P. Koshelets, and A. V. Ustinov, Nat. Phys. **6**, 593 (2010).
[27] F. Ando, Y. Miyasaka, T. Li, J. Ishizuka, T. Arakawa, Y. Shiota, T. Moriyama, Y. Yanase, and T. Ono, Nature (London) **584**, 373 (2020).
[28] L. Bauriedl, C. Bäuml, L. Fuchs, C. Baumgartner, N. Paulik, J. M. Bauer, K.-Q. Lin, J. M. Lupton, T. Taniguchi, K. Watanabe, C. Strunk, and N. Paradiso, Nat. Commun. **13**, 4266 (2022).
[29] J. Yun, S. Son, J. Shin, G. Park, K. Zhang, Y. J. Shin, J.-G. Park, and D. Kim, Phys. Rev. Res. **5**, L022064 (2023).
[30] J.-X. Lin, P. Siriviboon, H. D. Scammell, S. Liu, D. Rhodes, K. Watanabe, T. Taniguchi, J. Hone, M. S. Scheurer, and J. Li, Nat. Phys. **18**, 1221 (2022).
[31] J. Díez-Mérida, A. Díez-Carlón, S. Y. Yang, Y.-M. Xie, X.-J. Gao, K. Watanabe, T. Taniguchi, X. Lu, K. T. Law, and D. K. Efetov, arXiv:2110.01067.
[32] R. S. Souto, M. Leijnse, and C. Schrade, Phys. Rev. Lett. **129**, 267702 (2022).
[33] S. Ilić and F. S. Bergeret, Phys. Rev. Lett. **128**, 177001 (2022).
[34] N. F. Q. Yuan and L. Fu, Proc. Natl. Acad. Sci. USA **119**, e2119548119 (2022).
[35] A. Daido, Y. Ikeda, and Y. Yanase, Phys. Rev. Lett. **128**, 037001 (2022).
[36] J. J. He, Y. Tanaka, and N. Nagaosa, New J. Phys. **24**, 053014 (2022).
[37] H. D. Scammell, J. I. A. Li, and M. S. Scheurer, 2D Mater. **9**, 025027 (2022).

[38] T. H. Kokkeler, A. Golubov, and F. S. Bergeret, Phys. Rev. B **106**, 214504 (2022).

[39] Y.-Y. Lyu, J. Jiang, Y.-L. Wang, Z.-L. Xiao, S. Dong, Q.-H. Chen, M. V. Milošević, H. Wang, R. Divan, J. E. Pearson, P. Wu, F. M. Peeters, and W.-K. Kwok, Nat. Commun. **12**, 2703 (2021).

[40] Y. Hou, F. Nichele, H. Chi, A. Lodesani, Y. Wu, M. F. Ritter, D. Z. Haxell, M. Davydova, S. Ilić, O. Glezakou-Elbert, A. Varambally, F. S. Bergeret, A. Kamra, L. Fu, P. A. Lee, and J. S. Moodera, Phys. Rev. Lett. **131**, 027001 (2023).

[41] J. Hu, C. Wu, and X. Dai, Phys. Rev. Lett. **99**, 067004 (2007).

[42] D. Wang, Q.-H. Wang, and C. Wu, arXiv:2209.12646.

[43] Y. Zhang, Y. Gu, P. Li, J. Hu, and K. Jiang, Phys. Rev. X **12**, 041013 (2022)

[44] T. Karabassov, I. V. Bobkova, A. A. Golubov, and A. S. Vasenko, Phys. Rev. B **106**, 224509 (2022).

[45] K. Halterman, M. Alidoust, R. Smith, and S. Starr, Phys. Rev. B **105**, 104508 (2022).

[46] A. Daido and Y. Yanase, Phys. Rev. B **106**, 205206 (2022).

[47] B. Zhai, B. Li, Y. Wen, F. Wu, and J. He, Phys. Rev. B **106**, L140505 (2022).

[48] H. Narita, J. Ishizuka, R. Kawarazaki, D. Kan, Y. Shiota, T. Moriyama, Y. Shimakawa, A. V. Ognev, A. S. Samardak, Y. Yanase, and T. Ono, Nat. Nanotechnol. **17**, 823 (2022).

[49] M. Nadeem, M. S. Fuhrer, and X. Wang, arXiv:2301.13564.

[50] B. Pal, A. Chakraborty, P. K. Sivakumar, M. Davydova, A. K. Gopi, A. K. Pandeya, J. A. Krieger, Y. Zhang, S. Ju, N. Yuan, N. B. Schröter, L. Fu, and S. S. P. Parkin, Nat. Phys. **18**, 1228 (2022).

[51] M. Davydova, S. Prembabu, and L. Fu, Sci. Adv. **8**, eabo0309 (2022).

[52] C. Baumgartner, L. Fuchs, A. Costa, S. Reinhardt, S. Gronin, G. C. Gardner, T. Lindemann, M. J. Manfra, P. E. Faria Junior, D. Kochan, J. Fabian, N. Paradiso, and C. Strunk, Nat. Nanotechnol. **17**, 39 (2022).

[53] E. Bocquillon, R. S. Deacon, J. Wiedenmann, P. Leubner, T. M. Klapwijk, C. Brüne, K. Ishibashi, H. Buhmann, and L. W. Molenkamp, Nat. Nanotechnol. **12**, 137 (2017).

[54] B. Turini, S. Salimian, M. Carrega, A. Iorio, E. Strambini, F. Giazotto, V. Zannier, L. Sorba, and S. Heun, Nano Lett. **22**, 8502 (2022).

[55] K. Misaki and N. Nagaosa, Phys. Rev. B **103**, 245302 (2021).

[56] H. Wu, Y. Wang, P. K. Sivakumar, C. Pasco, S. S. Parkin, Y.-J. Zeng, T. McQueen, and M. N. Ali, Nature (London) **604**, 653 (2022).

[57] M. Gupta, G. V. Graziano, M. Pendharkar, J. T. Dong, C. P. Dempsey, C. Palmstrøm, and V. S. Pribiag, Nat. Commun. **14**, 3078 (2023).

[58] Y.-M. Xie, D. K. Efetov, and K. T. Law, Phys. Rev. Res. **5**, 023029 (2023).

[59] Y.-J. Wei, H.-L. Liu, J. Wang, and J.-F. Liu, Phys. Rev. B **106**, 165419 (2022).

[60] X. Sun, K.-H. Wu, R. Sakamoto, T. Kusamoto, H. Maeda, and H. Nishihara, Chem. Lett. **46**, 1072 (2017).

[61] A. Wang, X. Zhao, M. Zhao, X. Zhang, Y. Feng, and F. Liu, J. Phys. Chem. Lett. **9**, 614 (2018).

[62] C. L. Kane and E. J. Mele, Phys. Rev. Lett. **95**, 226801 (2005).

[63] V. Braude and Y. V. Nazarov, Phys. Rev. Lett. **98**, 077003 (2007).

[64] P.-H. Fu, Y. Xu, X.-L. Yu, J.-F. Liu, and J. Wu, Phys. Rev. B **105**, 064503 (2022).

[65] X. Zhou, Phys. Rev. B **104**, 125441 (2021).

[66] J. Wang, L. Hao, and J.-F. Liu, Phys. Rev. B **93**, 155405 (2016).

[67] H. Ren, F. Pientka, S. Hart, A. T. Pierce, M. Kosowsky, L. Lunczer, R. Schlereth, B. Scharf, E. M. Hankiewicz, L. W. Molenkamp, B. I. Halperin, and A. Yacoby, Nature (London) **569**, 93 (2019).

[68] A. Fornieri, A. M. Whiticar, F. Setiawan, E. Portolés, A. C. C. Drachmann, A. Keselman, S. Gronin, C. Thomas, T. Wang, R. Kallaher, G. C. Gardner, E. Berg, M. J. Manfra, A. Stern, C. M. Marcus, and F. Nichele, Nature (London) **569**, 89 (2019).

[69] S. Hart, H. Ren, T. Wagner, P. Leubner, M. Mühlbauer, C. Brüne, H. Buhmann, L. W. Molenkamp, and A. Yacoby, Nat. Phys. **10**, 638 (2014).

[70] C. Li, Y.-F. Zhao, A. Vera, O. Lesser, H. Yi, S. Kumari, Z. Yan, C. Dong, T. Bowen, K. Wang, H. Wang, J. L. Thompson, K. Watanabe, T. Taniguchi, D. R. Hickey, Y. Oreg, J. A. Robinson, C.-Z. Chang, and J. Zhu, Nat. Mater. **22**, 570 (2023).

[71] C.-Z. Chen, J. J. He, M. N. Ali, G.-H. Lee, K. C. Fong, and K. T. Law, Phys. Rev. B **98**, 075430 (2018).

[72] G. Tkachov, P. Burset, B. Trauzettel, and E. M. Hankiewicz, Phys. Rev. B **92**, 045408 (2015).

[73] F. Dolcini, M. Houzet, and J. S. Meyer, Phys. Rev. B **92**, 035428 (2015).